

RESEARCH ARTICLE

Open Access



# High-resolution analysis of multi-copy variant surface glycoprotein gene expression sites in African trypanosomes

Sebastian Hutchinson<sup>1</sup>, Lucy Glover<sup>1,2</sup> and David Horn<sup>1\*</sup>

## Abstract

**Background:** African trypanosomes cause lethal diseases in humans and animals and escape host immune attack by switching the expression of Variant Surface Glycoprotein (VSG) genes. The expressed VSGs are located at the ends of telomeric, polycistronic transcription units known as VSG expression sites (VSG-ESs). Each cell has many VSG-ESs but only one is transcribed in bloodstream-form parasites and all of them are inactive upon transmission to the insect vector mid-gut; a subset of monocistronic metacyclic VSG-ESs are then activated in the insect salivary gland. Deep-sequence analyses have been informative but assigning sequences to individual VSG-ESs has been challenging because they each contain closely related expression-site associated genes, or *ESAGs*, thought to contribute to virulence.

**Results:** We utilised ART, an *in silico* short read simulator to demonstrate the feasibility of accurately aligning reads to VSG-ESs. Then, using high-resolution transcriptomes from isogenic bloodstream and insect-stage Lister 427 *Trypanosoma brucei*, we uncover increased abundance in the insect mid-gut stage of mRNAs from metacyclic VSG-ESs and of mRNAs from the unusual *ESAG*, *ESAG10*. Further, we show that the silencing associated with allelic exclusion involves repression focussed at the ends of the VSG-ESs. We also use the approach to report relative fitness costs following *ESAG* RNAi from a genome-scale screen.

**Conclusions:** By assigning sequences to individual VSG-ESs we provide new insights into VSG-ES transcription control, allelic exclusion and impacts on fitness. Thus, deeper insights into the expression and function of regulated multi-gene families are more accessible than previously anticipated.

**Keywords:** Allelic exclusion, Antigenic variation, Gene expression, RNA-seq, *Trypanosoma brucei*, VSG

## Background

African trypanosomes are protozoan parasites that cause devastating diseases known as human African trypanosomiasis and a livestock disease known as nagana. These parasites are transmitted by the bite of an infected tsetse-fly, the distribution of which restricts the geographic spread of the disease. The parasite exists extracellularly, and is continually exposed to immune attack in the mammalian host [1]. To persist in the host bloodstream, the parasite has evolved a sophisticated strategy of antigenic variation and immune evasion. The trypanosome surface is coated in a dense layer of

$10^7$  copies of a single variant surface glycoprotein (VSG) [2]. Switching of this VSG coat is central to adaptive immune evasion, and operates at a rate of approximately  $10^{-6}$  per parasite cell division in culture [3]. In vivo, this leads to the recrudescence parasitaemia characteristic of *T. brucei* infection [1], where unswitched parasites are removed by antibody mediated killing.

VSG expression sites (VSG-ESs) are the key subtelomeric polycistronic units involved in antigenic variation in bloodstream African trypanosomes [4]. Understanding the expression and function of these units is critical to understanding virulence. VSG-ES transcription, mediated by RNA polymerase I, initiates at multiple VSG-ES promoters but is attenuated in all but one to prevent multi-VSG expression in individual

\* Correspondence: d.horn@dundee.ac.uk

<sup>1</sup>Division of Biological Chemistry & Drug Discovery, School of Life Sciences, University of Dundee, Dow Street, Dundee DD1 5EH, UK

Full list of author information is available at the end of the article



cells [5]. The polycistronic *VSG*-ESs contain a number of Expression Site Associated Genes (*ESAGs*), several of which are of unknown function, but those that have been characterised are involved in nutrient acquisition; *ESAG6* and *ESAG7* [6], and innate immune evasion; *ESAG4* and *SRA* [7, 8]. In trypanosomes, maturation of mRNA from nascent transcripts occurs via the linked processes of *trans*-splicing, the addition of a 39-nt capped leader sequence, and poly-adenylation [9, 10]. RNA Pol-II transcribes the spliced leader from a repetitive array as a primary 135 b transcript [11], that is processed and 5' capped before association with the spliceosome [12], which mediates *trans*-splicing to nascent transcripts [10].

Antigenic variation is specifically required for immune evasion in the bloodstream and, consistent with this, *VSG*-ESs are subject to developmental regulation. Upon parasite differentiation in the tsetse mid-gut, *VSG* transcription stops and the *VSG* coat is shed in the fly mid-gut, where recent evidence shows it interferes with fly innate immunity [13]. Procyclins, a family of repetitive proteins containing either EP or *GPEET* amino acid repeats, replace the *VSG* coat in the mid-gut [14]. Following migration to the fly salivary gland, a distinct sub-set of *VSGs* are expressed on the surface of metacyclic cells from monocistronic *VSG*-ESs, and are required for re-infection of the mammalian host [15, 16].

Next-generation sequencing (NGS) and RNA-seq approaches in particular, have been used in African trypanosomes to examine a range of features of genome organisation and gene expression, including developmentally regulated transcript expression [17], alternative splicing [18], control by RNA-binding proteins [19] and translation control [20, 21]. The approach has also been used to analyse relative expression levels for transcripts mapping to the active *VSG*-ES, revealing that most *ESAG* transcripts are present at 1–0.01 % the level of the active *VSG* transcript [17, 18].

NGS analysis of *VSG*-ESs presents several unique challenges. In particular, *VSG*-ESs are closely related [22] and, although increased mapping stringency can improve the alignment [23], the accuracy of assigning sequence-reads to the correct and specific sites has not been assessed in detail. Genes related to *ESAGs* (*GRESAGs*) are also found at non-telomeric locations; copies of *GRESAG4* are particularly prevalent and copies of *GRESAG2* are present at *procyclin* loci [24, 25]. In addition, *VSG*-ESs are under-represented in reference genome-sequence assemblies. Fortunately, the full set of *VSG*-ESs have been isolated and sequenced [22], and the subset of *VSG*-ESs expressed in the metacyclic stage has also been identified [15, 26], in the widely studied Lister 427 strain. However, developmental control of *VSG*-ESs has not yet been analysed in any detail in this strain.

We generated transcriptome data from sub-cloned populations of Lister 427 cells expressing a defined *VSG* (*VSG-2*) and from differentiated insect mid-gut stage cultures directly derived from those sub-clones. We then developed computational approaches to determine how accurately short reads derived from NGS can be aligned to *VSG*-ESs. We find that the differences between *VSG*-ESs are sufficient to allow 100-b reads to be accurately aligned to specific loci. Subsequent high-stringency mapping revealed a number of unanticipated features regarding *VSG*-ESs and their developmental control. High-stringency mapping was also applied to published NGS datasets. This revealed specific perturbations to *VSG*-ES transcriptomes following knockdown or over-expression of the allelic exclusion regulator *VEX1* [27], and relative fitness costs following knockdown of individual *ESAGs* [28].

## Results

### Transcriptomes from isogenic bloodstream and insect-stage *T. brucei*

We derived transcriptomes from a pair of Lister 427 bloodstream form sub-clones expressing *VSG-2* and from directly derived, differentiated, insect-stage cultures, separated from the bloodstream form sub-clones by only 10 days. Since the core, non sub-telomeric portion of the TREU-927 reference and Lister 427 genomes are closely related, sequence reads were aligned to the 11 megabase chromosomes from the TREU-927 genome [29], plus a non-redundant set of the 14 *VSG*-ESs [22] and 5 metacyclic *VSG*-ESs [15] from the Lister 427 strain. We aligned 26.4 and 26.5 million bloodstream form and 49.9 and 53.5 million insect-stage, 100 b, paired end reads using Bowtie2 [30], yielding approximately 180x genome coverage for bloodstream form and 350x for insect-stage transcriptomes. We calculated reads per kilobase of transcript per million mapped reads (RPKM), and differential expression using edgeR [31]; an additional table file shows these values (Additional file 1, 'BSF v PCF mapq > 0' tab). This revealed excellent reproducibility between clones, Pearson correlation coefficients of > 0.99 (Additional file 2), and robust developmental control of known bloodstream-form and insect-stage specific genes (Fig. 1a). For example, upon differentiation, the *EP* and *GPEET* procyclins increased 306 (EP1 and EP2 average) and 153-fold, respectively, while *VSG-2* decreased  $1.2 \times 10^6$  fold; *BES1* *ESAG* transcripts were also decreased (Fig. 1a). In addition, phosphoglycerate kinase A (PGKA) displayed little change while PGKB increased (3.3-fold) and PGKC decreased (4.7-fold), as expected [32].

We next analysed reads from bloodstream and insect-stage cells that aligned to the active *VSG*-ES. A single base resolution *BES1* plot (Fig. 1b) revealed a strikingly

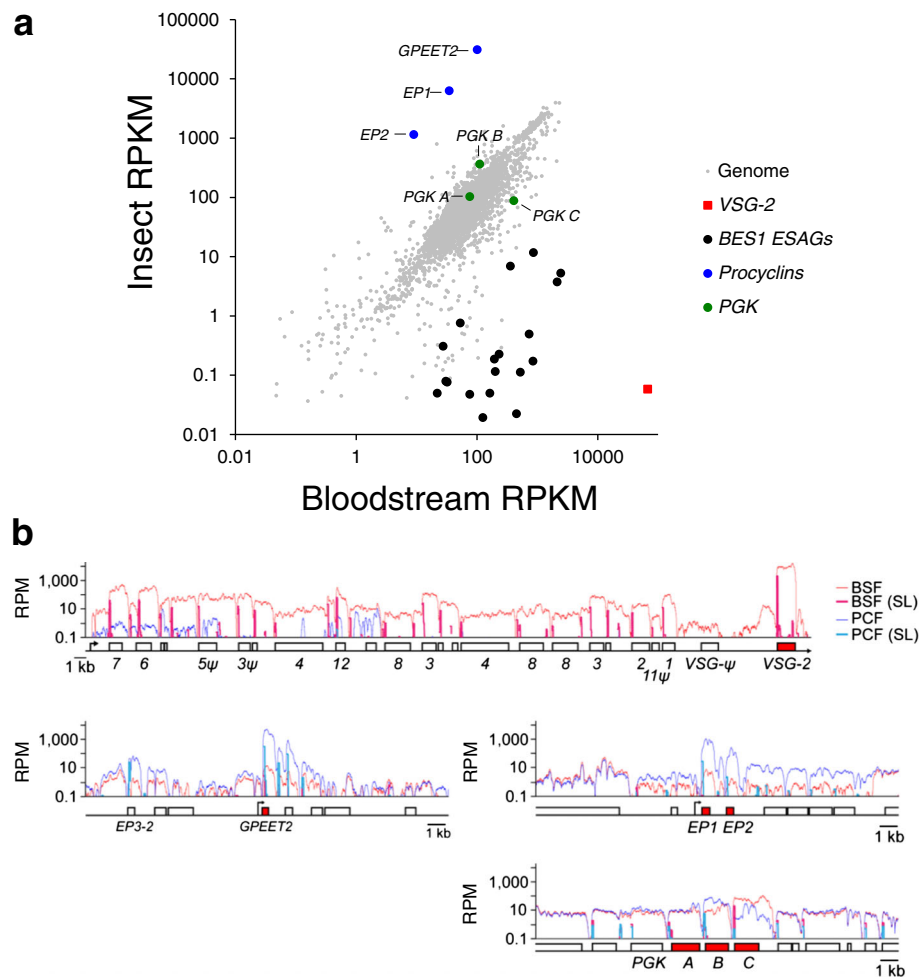


**Fig. 1** *T. brucei* transcriptomes from isogenic bloodstream and insect stage cultures. **a** The scatter plot shows RNA-seq data for bloodstream form and insect stage cultures. Values are calculated as RPKM (Reads Per Kilobase of transcript per Million mapped reads) and are averages for a pair of independent sub-clones. Selected developmentally regulated genes are highlighted. **b** Base-pair resolution plots of the active VSG-ES (top panel), *GPEET2* and *EP1/EP2* loci (middle panels) and the phosphoglycerate kinase locus (lower panel). Read counts are normalised using reads per million mapped (RPM) and trans-spliced reads are also indicated. Beneath each panel is a schematic map for each locus. Boxes, coding sequences; arrowheads, Pol-I promoters

compact transcription-unit, incorporating little inter-transcript DNA sequence. Reads associated with a trans-spliced leader sequence, found associated with all trypanosomatid mRNAs [10], revealed trans-splicing at discrete points for each gene (Fig. 1b), as expected [33]. We observed multiple trans-splicing events within the VSG gene, but the dominant splice-site was used >1000-fold more frequently than other sites. As also expected, we see bloodstream-specific over-representation (266 fold on average) of transcripts for every ESAG present in the active VSG-ES (Fig. 1b), consistent with transcription attenuation following differentiation [34]. In the bloodstream-form, the VSG transcript itself is 141-fold more abundant than the mean value of the other VSG-ES-derived transcripts. We do see some isolated ESAGs that display higher expression relative to

upstream ESAGs following differentiation to the insect stage but, rather than VSG-ES internal transcription initiation, this likely reflects incorrect assignment of reads from GRESAGs that are transcribed by RNA pol-II [24, 25]. Analysis of *procyclin* loci (also transcribed by RNA Pol-I) and the PGK locus (transcribed by RNA Pol-II) revealed similarly compact transcription units and the expected developmental controls (Fig. 1b). Thus, our RNA-seq datasets from isogenic bloodstream and insect-stage cultures are suitable for more detailed VSG-ES transcriptome analysis.

#### 'Short' reads can be accurately assigned to VSG-ESs

We next considered the challenge of accurately assigning 100-b sequence reads from RNA-seq datasets to individual VSG-ESs. Analysis of ESAG7 genes from the Lister

427 strain highlighted the challenge in terms of distinguishing among individual *ESAGs* (Additional file 3). In this case, a high level of identity was observed throughout the coding-sequence. There are differences however, which can be exploited.

In order to determine the feasibility of accurate short read alignment to *VSG-ESs*, we used ART [35] to simulate the Illumina sequencing platform *in silico* and to generate  $10^5$  single end, 100-b reads derived exclusively from individual *VSG-ESs*. We initially simulated Illumina sequencing runs of the sequence isolated from the active *VSG-ES* in our experimental strain and from three additional *VSG-ESs* (Fig. 2a). These reads were then aligned to the *VSG-ES* sequences using Bowtie2 [30], with the same settings used above. We observed reads aligning inappropriately to other *VSG-ESs*, however the signal to noise ratio could be increased significantly by

filtering reads by the uniqueness (MapQ value) of the alignment, assigned to each read by Bowtie2 (Fig. 2a). This filters reads with a higher probability of being mis-aligned to the genome. We went on to repeat this *in silico* analysis with the entire set of assembled bloodstream and metacyclic *VSG-ESs* from the Lister 427 strain (Fig. 2b).

The analysis indicated that Bowtie2 aligns 75.5 % of *in silico* generated reads to the correct bloodstream *VSG-ES* with a MapQ  $\geq 0$  (98.7 % to metacyclic *VSG-ESs*) such that mis-aligned reads, as expected, can have a significant negative impact on transcriptome analysis. A MapQ value of  $> 1$  removes 99.9 % of inappropriately aligned reads and retains 81 % of the signal while a MapQ  $> 12$  eradicated all noise from the data and retained 65.7 % of the signal (Fig. 2b). We selected a MapQ cutoff  $> 1$  as optimal for accurately assigning

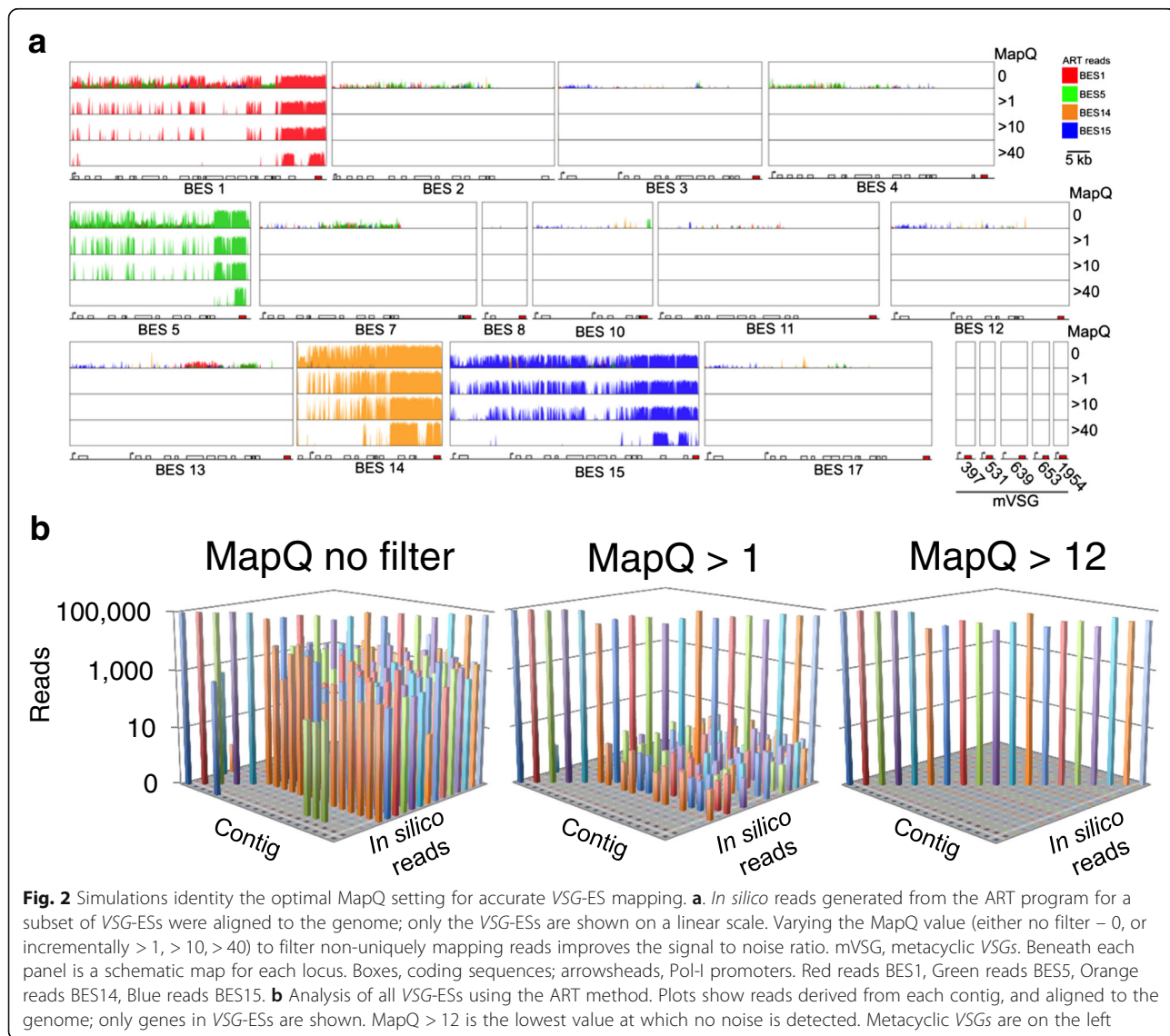


**Fig. 2** Simulations identify the optimal MapQ setting for accurate *VSG-ES* mapping. **a.** *In silico* reads generated from the ART program for a subset of *VSG-ESs* were aligned to the genome; only the *VSG-ESs* are shown on a linear scale. Varying the MapQ value (either no filter – 0, or incrementally  $> 1$ ,  $> 10$ ,  $> 40$ ) to filter non-uniquely mapping reads improves the signal to noise ratio. mVSG, metacyclic *VSGs*. Beneath each panel is a schematic map for each locus. Boxes, coding sequences; arrowheads, Pol-I promoters. Red reads BES1, Green reads BES5, Orange reads BES14, Blue reads BES15. **b** Analysis of all *VSG-ESs* using the ART method. Plots show reads derived from each contig, and aligned to the genome; only genes in *VSG-ESs* are shown. MapQ  $> 12$  is the lowest value at which no noise is detected. Metacyclic *VSGs* are on the left

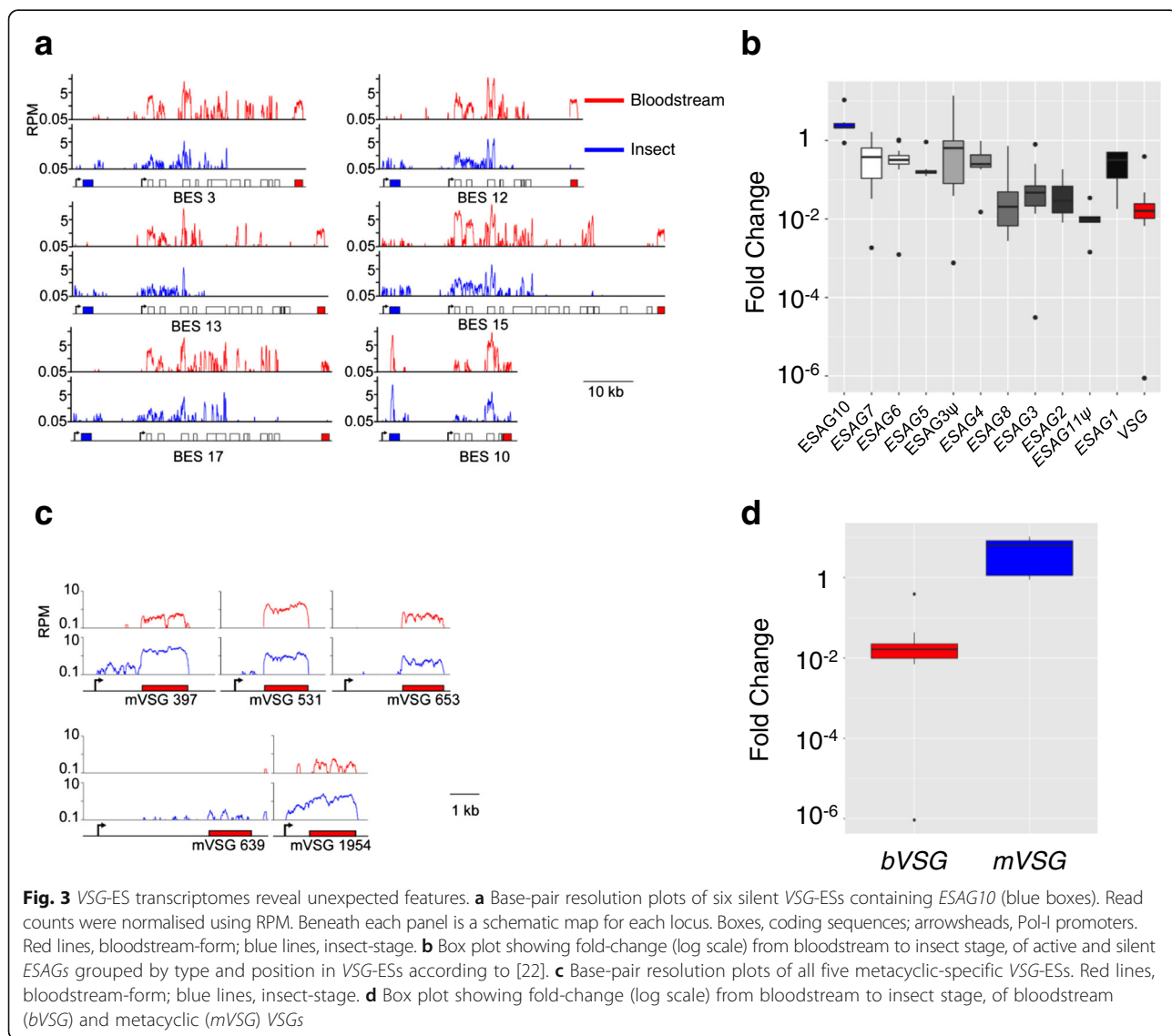
short sequence reads to individual *VSG*-ESs; the vast majority of *VSG*-ES associated genes retain short reads using this approach; an additional table file shows these values (Additional file 1, 'BSF v PCF mapq > 1' tab).

During this analysis, we also observed a distinct trend in the distribution of *in silico*-generated reads. Specifically, reads were more effectively retained closer to the telomere as we increased the uniqueness of alignment (Additional file 4A), indicating that sequences closer to telomeres are more divergent/unique. The alignment map for promoter-proximal *ESAG7* genes from Additional file 3 is also compared to an alignment map for the telomere-proximal *ESAG1* to further illustrate this point (Additional file 4B). Although a contested hypothesis [36], error-prone *VSG* gene-conversion was previously suggested as a mechanism contributing to antigenic variation [37, 38]. Our observation is consistent with this

hypothesis when taken together with the inherent fragility of sub-telomeres and subsequent telomere-directed gene-conversion events [39].

**Differential controls affecting specific *ESAGs* and *VSGs***

Using a MapQ > 1, we filtered our RNA-seq data for high-confidence read alignments to *VSG*-ESs. The major developmental changes reported above (Fig. 1a) were also observed for this filtered dataset (Additional file 5). Filtering allowed us to assign reads to 'silent' *VSG*-ESs (Fig. 3a-b) and this revealed transcripts originating from the majority of *VSGs* in bloodstream-form cells (Additional file 5). This may reflect low-level expression of other *VSG*-ESs in cells expressing *VSG-2* or may equally reflect low-frequency activation of alternate *VSG*-ESs. Since our RNA samples were prepared using approximately 100 million cells and switching



occurs in approximately one in every  $10^6$  cells, we expect approximately 100 distinct switching events to be represented, although this does not so readily explain the expression of metacyclic *VSG* genes. As transcription is initiated at all *VSG*-ESs [5], proximity to the promoter may explain this low-level transcription of metacyclic *VSGs* that we observe in bloodstream form cells (Fig. 3c).

Reads mapping to ‘silent’ *VSG*-ESs are  $2.4 \times 10^4$ -fold lower on average relative to those mapping to the active *VSG*-ES and are further reduced when cells differentiate to the insect stage (Fig. 3a). Again, we see some isolated *ESAGs* that display higher expression relative to upstream genes, likely reflecting reads from RNA pol-II transcribed *GRESAGs* [24, 25]. *VSG*-ESs share a generic structure, with similar *ESAGs* in similar positions. When grouped and represented according to their position, *VSG*-ES associated genes closer to telomeres display greater down-regulation in the insect-stage (Fig. 3b). For instance, average *VSG* expression level decreases 21-fold upon differentiation to insect stage cells, while *ESAG7* expression decreased only 2 fold. In contrast to other *ESAGs*, four of six *ESAG10* genes were significantly ( $p < 0.05$ ) upregulated (average 3.9 fold) in the insect-stage (Fig. 3a-b). This was unexpected since *ESAG* expression has been considered bloodstream stage-specific [40]. Thus, *ESAG10* may be an unconventional *ESAG* in terms of developmental expression-control.

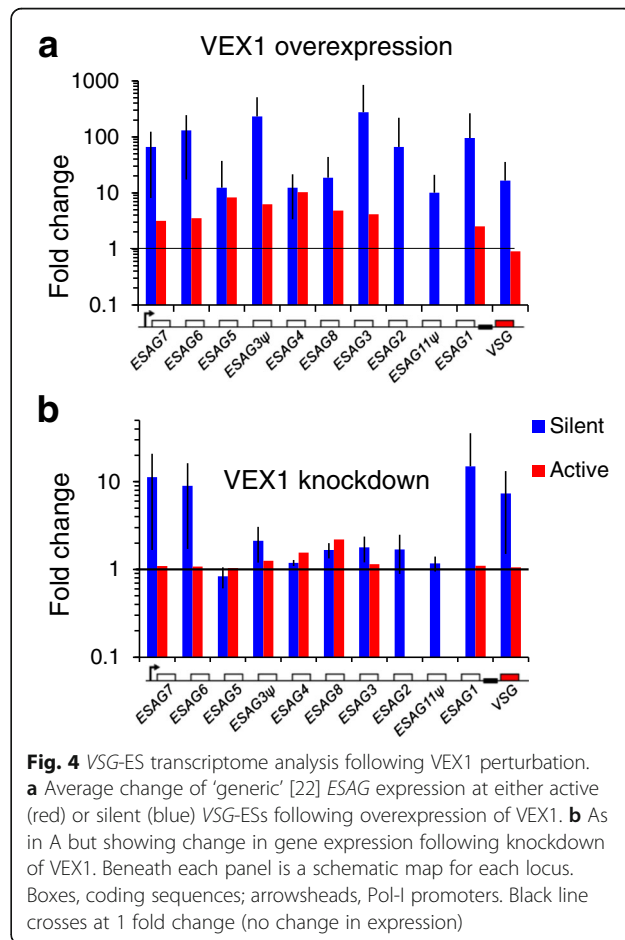
Another unexpected observation was that, while *VSGs* in polycistronic *VSG*-ESs were down-regulated, three of the five *VSGs* located within the monocistronic metacyclic *VSG*-ESs were expressed at a significantly higher level (8.4 fold average,  $p < 10^{-22}$ ) in insect-stage cells (Fig. 3c-d, Additional file 5). *VSG* expression has been considered to be specific to the tsetse salivary gland stage and the bloodstream-stages, due to promoter control (the *VSG*-ES promoters active in bloodstream-form cells are distinct from the *VSG* promoters active in metacyclic cells) and stage-specific stabilisation of transcripts driven by a conserved element in the *VSG* mRNA 3’ untranslated sequence [41]. We speculate that the unexpected increase in expression of monocistronic metacyclic *VSGs* reflects progression to a metacyclic (–like) stage by small numbers of cells present in differentiated cultures. Indeed, increased expression of a single RNA binding-protein, RBP6, can trigger this progression through the life cycle [15]. Alternatively, sub-telomeric silencing may be less pronounced in insect-stage cells.

Our analysis of silent *VSG*-ESs allowed us to identify the *trans*-splicing sites for twelve *VSG*-ES linked *VSGs* and all five metacyclic *VSGs* from our RNA-seq data (Additional file 6A-B). We counted polypyrimidine tract lengths for *VSG* splice sites and compared these to the

genes in the RNA Pol-I transcribed *procyclin* loci, counting the number of consecutive pyrimidines and allowing for a single purine interruption. We found that the *VSG* genes are associated with significantly shorter polypyrimidine tracts (11.5 b,  $n = 17$ ) compared to genes in the *procyclin* loci (19.0 b,  $n = 13$ ,  $p < 4 \times 10^{-4}$ ) or the 20 most abundant RNA Pol-II transcripts in our dataset (20.4 b,  $n = 20$ ,  $p < 5 \times 10^{-4}$ ) (Additional file 6C). Notably, *ESAG7* genes also possess shorter polypyrimidine tracts, suggesting that *VSG*-ES associated genes do not require extensive polypyrimidine tracts to form abundant mature messenger RNAs. Identification of splice-sites also allowed us to predict 5’-untranslated sequences and we note that there does not appear to be a consensus here; these sequences range in size from 15 to 91 b.

#### Regulation of *VSG*-ES transcripts by VEX1

VEX1 (VSG exclusion 1) is an allelic exclusion regulator required for the control of *VSG* gene expression [27]. In order to further our understanding of control by VEX1, we analysed the RNA-seq datasets generated following VEX1 overexpression (Fig. 4a) or RNAi knockdown (Fig. 4b), which both lead to increased expression of

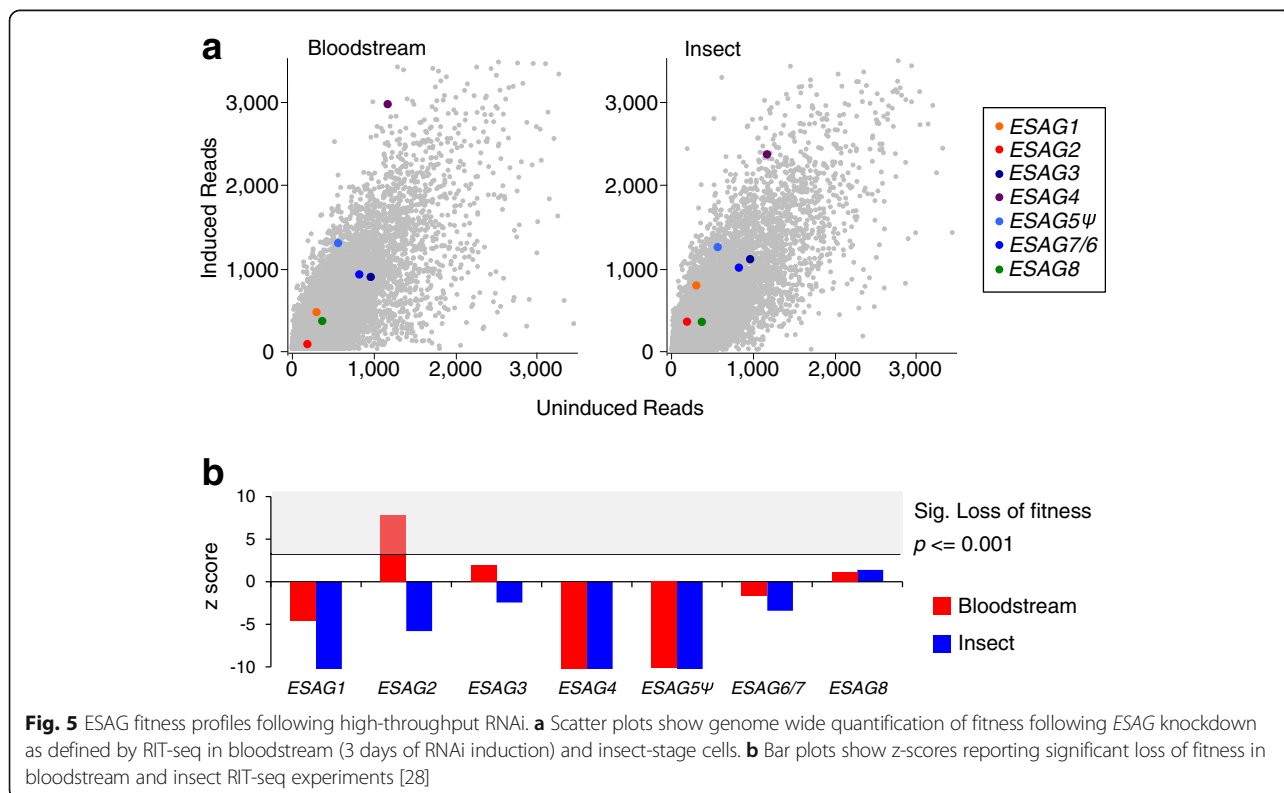


‘silent’, ES-associated *VSG* genes [27]; an additional table file shows these values (Additional file 1, ‘VEX1’ tabs). High confidence (MapQ > 1) read alignments, of genes with > 10 reads when VEX1 was overexpressed, revealed an average of 5.4 fold more active *VSG-ES ESAG* transcripts, with 77 % of genes tested significantly increasing (> 3 fold change,  $p < 0.05$ ) (Fig. 4a, Additional file 7, red bars), and an average 93-fold increase in silent *ESAG* transcripts, with 86 % of genes tested increasing significantly (> 3 fold change,  $p < 0.05$ ) (Fig. 4a, Additional file 7, blue bars). These results are consistent with the previously reported positive control by ectopically expressed VEX1 [27].

We next analysed the RNA-seq data derived following VEX1 RNAi (Fig. 4b, Additional file 7). In this case, our analysis shows minimal impact at the active *VSG-ES* (Fig. 4b, red bars) but differential behaviour of the ‘silent’ *VSGs* and the *ESAGs* at either end of *VSG-ESs* relative to the centrally located *ESAGs*. Specifically, the promoter-adjacent *ESAG6* and *7* were increased 10-fold; 75 % of genes tested increasing significantly (> 3 fold,  $p < 0.05$ ), while the telomere-proximal *VSG* and *ESAG1* increased 10 to 15-fold; 50 % of genes tested increasing significantly (> 3 fold,  $p < 0.05$ ). This is in contrast to several centrally located *ESAGs*, which increased only 1.5 fold on average, with just 2 % of genes tested increasing significantly (> 3 fold,  $p < 0.05$ ).

**Loss-of-fitness associated with *ESAG* knockdown**

Our understanding of the functions of the *ESAGs* remains incomplete and, because of difficulties with accurate mapping as outlined above, the *ESAGs* were not analysed as part of prior high-throughput phenotyping analysis using RNA interference (RNAi) in *in vitro* culture [28]. We revisited these data and mapped RIT-seq reads (MapQ > 1) from bloodstream and insect stage cells to the *VSG-ES* active in the bloodstream-form (Fig. 5a); an additional table file shows these values (Additional file 1, ‘BES1 RIT-seq’ tab). Although the RNAi library used in the Lister 427 strain was derived from the TREU 927 strain, the closely related RNAi target fragments are still expected to mediate efficient *ESAG* knockdown [42]. Mapped reads were quantified and analysed relative to the uninduced control (Fig. 5b) revealing loss-of-fitness following *ESAG2*, *ESAG3* and *ESAG8* RNAi that achieved significance following *ESAG2* RNAi; other *ESAGs* failed to register a loss-of-fitness. A previous study reported loss-of-fitness for every *ESAG* knockdown tested [43] but *ESAG2* also registered the greatest loss-of-fitness in that study. This phenotype may reflect the knockdown of RNA pol-II transcribed *GRESAG2* transcripts [24, 25] rather than *VSG-ES* associated *ESAG2* transcripts, however. None of the *ESAGs*, except for *ESAG8*, registered a loss-of-fitness in the insect-stage, consistent with developmental stage-



specific *ESAG* expression. Notably, several *ESAGs* may be specifically required for host-parasite interactions, functions that are dispensable in *in vitro* culture.

## Discussion

Massive parallel NGS approaches have revolutionised the study of gene regulation and expression, producing data with an unrivalled depth [44], and have been applied with great success in African trypanosomes; see [17, 18, 33] for just a few examples. There are, however, a number of challenges associated with the analysis of subtelomeric sequences in a range of eukaryotes. These regions often incorporate highly repetitive and plastic components of the genome. This is particularly true of parasites, in which subtelomeric genes function in the processes of antigenic variation and immune evasion, such as malaria parasites [45] and African trypanosomes [4].

Analysis of these repetitive loci has proven challenging, a fact exemplified by our *in silico* analyses. Indeed, we note the use of orthogonal methods such as qRT-PCR and genetic tagging of *VSG-ESs* [46, 47], despite the availability of NGS approaches and datasets. We now report high-coverage transcriptomes from isogenic *T. brucei* cultures and from two major life cycle stages, namely the mammal-infective bloodstream form and the tsetse fly mid-gut stage, with a focus on the regulation of *VSG-ES* transcription. Simulated Illumina sequence data allowed us to gauge an appropriate filter that maximises the signal-to-noise ratio of sequence alignments at these loci. We find the expected extreme developmental regulation of *VSG* and *EP/GPEET* surface antigen genes and *VSG-ES* attenuation in insect stage cells but also, using high-stringency mapping, uncover additional and unexpected features.

Previous reports indicate that alignment of short reads to *VSG-ESs* can be problematic due to the similarity between these loci [22, 46, 48]. Our analyses show that an average of 24.5 % of *VSG-ES* derived reads are typically incorrectly aligned to *VSG-ESs*, and filtering reads with a MapQ value > 1 greatly reduces mis-mapping. Further analyses of *VSG-ESs* suggest that this is particularly useful for the closely related *ESAG* sequences. Improvements in sequencing technologies, such as quality (our sequence data has mean per-base quality scores > 34) and read-length now facilitate accurate high-stringency mapping. Specifically, we believe that 100–150 b reads that are commonly produced by current Illumina technologies incorporate sufficient SNPs to allow specific assignment to individual *VSG-ESs*.

In bloodstream cells, monoallelic expression ensures that a single subtelomere is productively transcribed [1]. However, in mid-gut stage cells, *VSG-ESs* are silenced [34]. In our populations, we find that transcripts for twelve silent *VSG-ES* linked and all five metacyclic *VSGs*

are detectable, although at a level approximately 26,000 times lower than the active *VSG*; illustrating the impressive dynamic range of RNA-seq. In addition, our analysis reveals that *ESAG10* mRNAs, encoding putative folate transporters [49], are more abundant in the mid-gut stage cultures than the bloodstream form. This surprising finding is suggestive of less effective silencing in the insect-stage of *ESAG10*-associated *VSG-ES* promoters relative to the almost identical *VSG-ES* promoters located downstream [22]. Alternatively, *ESAG10* transcripts may display increased stability in insect-stage cells. Notably, additional RNA pol-II transcribed genes on chromosome 8 (Tb927.8.3620, 3630 and 3650) encode folate transporters and whether the *ESAG10*-associated promoters or transcripts are 'activated' at any point in the life cycle remains unknown.

High-stringency mapping using transcriptomic datasets derived following knockdown of the allelic exclusion regulator, VEX1 [27], revealed derepression of promoter and telomere proximal *VSG-ES* genes. In another study, ectopic overexpression of a second *VSG* gene resulted in *VSG-ES* silencing spreading from the telomere towards the promoter in a disruptor of telomeric silencing 1B (DOT1B) dependent manner [43]. Our analysis indicates that VEX1-mediated silencing is directed at the telomeric *VSG* and *ESAG1* genes, and at the *VSG-ES* promoter-adjacent *ESAG6* and *ESAG7* genes. This is in contrast to VEX1 overexpression, which upregulates all silent *ESAGs* and *VSGs*. Thus, our current data indicate that VEX1-mediated silencing primarily affects the ends of silent *VSG-ESs*, suggesting that subtelomere conformation may be important in the control of these genes. Finally, high-stringency phenotyping data confirm (*GR*)*ESAG2* as the *ESAG* associated with the greatest fitness cost when knocked-down in *in vitro* culture.

## Conclusions

By distinguishing between closely related transcription units, we have been able to enhance our understanding of the behaviour of *VSG-ESs* in terms of *VSG* silencing, developmental regulation and contributions to fitness in culture. NGS approaches, coupled to high-stringency mapping, such as RNA-seq, ChIP-seq, RIT-seq and the growing list of 'seq' technologies will undoubtedly improve our understanding of the organisation and expression of these virulence gene loci and indeed closely related gene families in a range of other organisms.

## Methods

### *T. brucei*

Two subclones of wild type bloodstream-form Lister 427 strain *T. brucei* expressing *VSG-2* (*VSG-221*, Mitat1.2) were differentiated in insect mid-gut stage cells as previously described [50]. Briefly, cells were collected by centrifugation



and resuspended in differentiation medium (DTM) [50] supplemented with 3 mM citrate and 3 mM cis-aconitate and maintained for 10 days at 27 °C, 0 % CO<sub>2</sub> (ambient).

### RNA-seq

For RNA extraction,  $5 \times 10^7$  cells were collected and RNA prepared using the Qiagen RNeasy kit, according to the manufacturer's instructions. Poly-A+ RNA was enriched using oligo-dT beads, and reverse transcribed. Second strand synthesis was randomly primed. Sequencing was performed on the HiSeq platform (Illumina) at the University of Dundee generating 100-b paired-end reads. This yielded insect-stage RNA-seq data, using identical processing, that were only 10-days removed from our bloodstream-form RNA-seq data [27].

In order to align reads we generated a hybrid genome assembly consisting of the 11 megabase chromosomes from the *T. brucei* 927 reference genome [29], the non-redundant set of 14 bloodstream expression sites [22] and the 5 metacyclic expression sites from our Lister 427 strain [15, 26]. Read alignment was performed using Bowtie2 [30] as previously described [27] using the parameters `-very-sensitive -no-discordant`. Approximately 25 million bloodstream-form and 50 million insect stage reads were aligned for each clone. Alignment files were manipulated using SAMtools [51], and visualized in the Artemis genome browser [52]. Single base resolution plots were generated using the pysam API (<https://github.com/pysam-developers/pysam>) in an in-house script that filters reads based on alignment quality (MapQ) and corrects for library size (available on request). Trans-spliced reads were extracted using a previously published script [53], using the partial spliced leader sequence 'TCTGTACTATATTG' and its reverse complement to search. This is the shortest sequence that returns only spliced leader sequences following BLAST search of the TREU-927 genome sequence on TriTrypDB. Differential expression analysis was performed with edgeR [31] as previously described [27]. When analysing VEX1 perturbation, we excluded genes with <10 reads averaged across replicates in both uninducing or inducing conditions.

### ART simulation

ART is a software package that simulates next-generation sequencing runs using empirical error models utilized by the 1000 genomes project [35]. Illumina sequencing runs were simulated for all 19 of the Lister 427 VSG-ES contigs in the hybrid genome using the parameters `art_illumina -i contigX.fa -len 100 -ss MS -c 100000`. This produced 10<sup>5</sup> single-end reads for each contig; as the longest contig is 59,781 bp, this provided coverage of every base in each VSG-ES. These *in silico* reads were then aligned back to the complete genome with Bowtie2 using the parameters `-very-sensitive` [30]. Alignment files were manipulated

using SAMtools [51]. Read counts were generated using the Artemis genome browser [52].

### Sequence and data analysis

Clustal alignment analysis and visualisation of *ESAG7* sequences was performed using CLC workbench using settings: gap open cost = 0.0, gap extension cost = 0.0, end gap cost = free, alignment mode = very accurate, redo alignments = no, use fixedpoints = yes. A non-redundant gene list was from [28] and VSG-ES sequences [22] were retrieved from TriTrypDB. 'Generic' *ESAG* lists are derived from [22]; *ESAGs* from each VSG-ES were compiled based on relative position within each VSG-ES.

### Additional files

**Additional file 1:** Table containing RNA-seq and RIT-seq data. (XLSX 3.97 mb)

**Additional file 2:** Comparison of RNA-seq replicates. Scatter plots of bloodstream-form and insect-stage RPKM values for each condition. Data used to derive plots in Fig. 1 (MapQ >=0). (PDF 213 kb)

**Additional file 3:** *ESAG7* sequences are highly similar between VSG-ESs. Clustal alignment between *ESAG7* nucleotide sequence in BES1 (Tb429.BES40.2) and other *ESAG7* sequences. BES2, 4 and 8 have multiple *ESAG7* genes. (PDF 39 kb)

**Additional file 4:** Divergence increases towards the telomere. A. RPKM values for each *ESAG* and VSG in the non-redundant set plotted against the distance from the start-codon to the telomere. B. *ESAG7* Clustal alignment plot from Additional file 3 compared to *ESAG1* Clustal alignment plot. (PDF 174 kb)

**Additional file 5:** High stringency RNA-seq analysis. Scatter plot of RPKM values of each condition with MapQ value > 1. Values are calculated as RPKM (Reads Per Kilobase of transcript per Million mapped reads) and are averages for a pair of independent sub-clones. Selected developmentally regulated genes are highlighted. Metacyclic (*mVSG*) and bloodstream (*bVSG*) specific VSGs are also shown. (PDF 242 kb)

**Additional file 6:** VSG genes have significantly shorter polypyrimidine tracts upstream. A. Logo plots of the 17 VSG *trans*-splice sites identified from our data set (top) and genes in the RNA Pol-I transcribed *procyclin* loci. Pyrimidines, red; purines, grey. B. Individual *trans*-splice sites from beta-tubulin (top), bloodstream VSG-ES linked VSGs and metacyclic VSGs. Pyrimidines, red; purines, grey. C. Bar charts show average polypyrimidine tract length comparisons over several gene groups. \*\*\*, *P* < 0.0005. (PDF 471 kb)

**Additional file 7:** Individual VSG-ES transcriptome analysis following VEX1 perturbation. Bar-charts show fold-changes for *ESAG* expression in each VSG-ES following either VEX1 knockdown (blue bars) or overexpression (red bars). (PDF 149 kb)

### Abbreviations

BES: Bloodstream expression site; BSF: Bloodstream form; bVSG: Bloodstream VSG; CHIP-seq: Chromatin immunoprecipitation sequencing; DOT1B: Disruptor of telomeric silencing 1B; DTM: Differentiation trypanosome medium; *ESAG*: Expression-site associated gene; *GRESAG*: Gene related to *ESAG*; mVSG: Metacyclic VSG; NGS: Next-generation sequencing; PCF: Procyclic (insect) form; PGK: Phosphoglycerate kinase; qRT-PCR: Quantitative reverse transcription polymerase chain reaction; RBP: RNA binding-protein; RIT-seq: RNA interference target sequencing; RNA Pol: RNA polymerase; RNAi: RNA interference; RNA-seq: RNA sequencing; RPKM: Reads per kilobase of transcript per million mapped reads; RPM: Reads per million mapped; SRA: Serum resistance-associated; TREU: Trypanosomiasis research Edinburgh University; VEX1: VSG exclusion 1; VSG: Variant surface glycoprotein; VSG-ES: VSG expression site

**Funding**

The work was supported by The Wellcome Trust (Investigator Award 100320/Z/12/Z to D.H. and Strategic Award 100476/Z/12/Z supporting Biological Chemistry & Drug Discovery).

**Availability of data and materials**

The RNA-seq sequence data reported in this paper have been deposited in the European Nucleotide Archive, www.ebi.ac.uk/ena (accession no. PRJEB8747). Genome sequences assembled from publicly available data (tritypdb.org) for this paper, and any scripts used are provided on request without condition.

**Authors' contributions**

SH and DH designed the study and analysed the data, LG generated samples for RNA-seq. SH, LG and DH wrote the paper. All authors read and approved the final manuscript.

**Competing interests**

The authors declare that they have no competing interests.

**Consent for publication**

Not applicable.

**Ethics approval and consent to participate**

Not applicable.

**Author details**

<sup>1</sup>Division of Biological Chemistry & Drug Discovery, School of Life Sciences, University of Dundee, Dow Street, Dundee DD1 5EH, UK. <sup>2</sup>Present address: Trypanosomes Molecular Biology, Institut Pasteur, 75015 Paris, France.

Received: 7 July 2016 Accepted: 11 October 2016

Published online: 18 October 2016

**References**

- Horn D. Antigenic variation in African trypanosomes. *Mol Biochem Parasitol.* 2014;195(2):123–9.
- Cross GA. Identification, purification and properties of clone-specific glycoprotein antigens constituting the surface coat of *Trypanosoma brucei*. *Parasitology.* 1975;71(3):393–417.
- Boothroyd CE, Dreesen O, Leonova T, Ly KI, Figueiredo LM, Cross GA, Papavasiliou FN. A yeast-endonuclease-generated DNA break induces antigenic switching in *Trypanosoma brucei*. *Nature.* 2009;459(7244):278–81.
- Glover L, Hutchinson S, Alsford S, McCulloch R, Field MC, Horn D. Antigenic variation in African trypanosomes: the importance of chromosomal and nuclear context in VSG expression control. *Cell Microbiol.* 2013;15(12):1984–93.
- Kassem A, Pays E, Vanhamme L. Transcription is initiated on silent variant surface glycoprotein expression sites despite monoallelic expression in *Trypanosoma brucei*. *Proc Natl Acad Sci U S A.* 2014;111(24):8943–8.
- Schell D, Evers R, Preis D, Ziegelbauer K, Kiefer H, Lottspeich F, Cornelissen AW, Overath P. A transferrin-binding protein of *Trypanosoma brucei* is encoded by one of the genes in the variant surface glycoprotein gene expression site. *EMBO J.* 1991;10(5):1061–6.
- Salmon D, Vanwalleghem G, Morias Y, Denoelud J, Krumbholz C, Lhomme F, Bachmaier S, Kador M, Gossmann J, Dias FB, et al. Adenylate cyclases of *Trypanosoma brucei* inhibit the innate immune response of the host. *Science.* 2012;337(6093):463–6.
- Xong HV, Vanhamme L, Chamekh M, Chimfwembe CE, Van Den Abbeele J, Pays A, Van Meirvenne N, Hamers R, De Baetselier P, Pays E. A VSG expression site-associated gene confers resistance to human serum in *Trypanosoma rhodesiense*. *Cell.* 1998;95(6):839–46.
- Matthews KR, Tschudi C, Ullu E. A common pyrimidine-rich motif governs trans-splicing and polyadenylation of tubulin polycistronic pre-mRNA in trypanosomes. *Genes Dev.* 1994;8(4):491–501.
- Parsons M, Nelson RG, Watkins KP, Agabian N. Trypanosome mRNAs share a common 5' spliced leader sequence. *Cell.* 1984;38(1):309–16.
- Milhausen M, Nelson RG, Sather S, Selkirk M, Agabian N. Identification of a small RNA containing the trypanosome spliced leader: a donor of shared 5' sequences of trypanosomatid mRNAs? *Cell.* 1984;38(3):721–9.
- Tschudi C, Ullu E. Destruction of U2, U4, or U6 small nuclear RNA blocks trans splicing in trypanosome cells. *Cell.* 1990;61(3):459–66.
- Aksoy E, Vigneron A, Bing X, Zhao X, O'Neill M, Wu YN, Bangs JD, Weiss BL, Aksoy S. Mammalian African trypanosome VSG coat enhances tsetse's vector competence. *Proc Natl Acad Sci U S A.* 2016;113(25):6961–6.
- Roditi I, Schwarz H, Pearson TW, Beecroft RP, Liu MK, Richardson JP, Buhning HJ, Pleiss J, Bulow R, Williams RO, et al. Procydin gene expression and loss of the variant surface glycoprotein during differentiation of *Trypanosoma brucei*. *J Cell Biol.* 1989;108(2):737–46.
- Koley NG, Ramey-Butler K, Cross GA, Ullu E, Tschudi C. Developmental progression to infectivity in *Trypanosoma brucei* triggered by an RNA-binding protein. *Science.* 2012;338(6112):1352–3.
- Sharma R, Gluenz E, Peacock L, Gibson W, Gull K, Carrington M. The heart of darkness: growth and form of *Trypanosoma brucei* in the tsetse fly. *Trends Parasitol.* 2009;25(11):517–24.
- Siegel TN, Hekstra DR, Wang X, Dewell S, Cross GA. Genome-wide analysis of mRNA abundance in two life-cycle stages of *Trypanosoma brucei* and identification of splicing and polyadenylation sites. *Nucleic Acids Res.* 2010;38(15):4946–57.
- Nilsson D, Gunasekera K, Mani J, Osteras M, Farinelli L, Baerlocher L, Roditi I, Ochsenreiter T. Spliced leader trapping reveals widespread alternative splicing patterns in the highly dynamic transcriptome of *Trypanosoma brucei*. *PLoS Pathog.* 2010;6(8):e1001037.
- Wurst M, Seliger B, Jha BA, Klein C, Queiroz R, Clayton C. Expression of the RNA recognition motif protein RBP10 promotes a bloodstream-form transcript pattern in *Trypanosoma brucei*. *Mol Microbiol.* 2012;83(5):1048–63.
- Jensen BC, Ramasamy G, Vasconcelos EJ, Ingolia NT, Myler PJ, Parsons M. Extensive stage-regulation of translation revealed by ribosome profiling of *Trypanosoma brucei*. *BMC Genomics.* 2014;15:911.
- Vasquez JJ, Hon CC, Vanselow JT, Schlosser A, Siegel TN. Comparative ribosome profiling reveals extensive translational complexity in different *Trypanosoma brucei* life cycle stages. *Nucleic Acids Res.* 2014;42(6):3623–37.
- Hertz-Fowler C, Figueiredo LM, Quail MA, Becker M, Jackson A, Bason N, Brooks K, Churcher C, Fahkro S, Goodhead I, et al. Telomeric expression sites are highly conserved in *Trypanosoma brucei*. *PLoS One.* 2008;3(10):e3527.
- Schulz D, Mugnier MR, Paulsen EM, Kim HS, Chung CW, Tough DF, Rioja I, Prinjha RK, Papavasiliou FN, Debler EW. Bromodomain proteins contribute to maintenance of bloodstream form stage identity in the African trypanosome. *PLoS Biol.* 2015;13(12):e1002316.
- Berberof M, Pays A, Pays E. A similar gene is shared by both the variant surface glycoprotein and procyclin gene transcription units of *Trypanosoma brucei*. *Mol Cell Biol.* 1991;11(3):1473–9.
- Paindavoine P, Rolin S, Van Assel S, Geuskens M, Jauniaux JC, Dinsart C, Huet G, Pays E. A gene from the variant surface glycoprotein expression site encodes one of several transmembrane adenylate cyclases located on the flagellum of *Trypanosoma brucei*. *Mol Cell Biol.* 1992;12(3):1218–25.
- Cross GA, Kim HS, Wickstead B. Capturing the variant surface glycoprotein repertoire (the VSGnome) of *Trypanosoma brucei* Lister 427. *Mol Biochem Parasitol.* 2014;195(1):59–73.
- Glover L, Hutchinson S, Alsford S, Horn D. VEX1 controls the allelic exclusion required for antigenic variation in trypanosomes. *Proc Natl Acad Sci U S A.* 2016;113:7225–30.
- Alsford S, Turner DJ, Obado SO, Sanchez-Flores A, Glover L, Berriman M, Hertz-Fowler C, Horn D. High-throughput phenotyping using parallel sequencing of RNA interference targets in the African trypanosome. *Genome Res.* 2011;21(6):915–24.
- Berriman M, Ghedin E, Hertz-Fowler C, Blandin G, Renaud H, Bartholomeu DC, Lennard NJ, Caler E, Hamlin NE, Haas B, et al. The genome of the African trypanosome *Trypanosoma brucei*. *Science.* 2005;309(5733):416–22.
- Langmead B, Salzberg SL. Fast gapped-read alignment with Bowtie 2. *Nat Methods.* 2012;9(4):357–9.
- Robinson MD, McCarthy DJ, Smyth GK. edgeR: a bioconductor package for differential expression analysis of digital gene expression data. *Bioinformatics.* 2010;26(1):139–40.
- Blattner J, Clayton CE. The 3'-untranslated regions from the *Trypanosoma brucei* phosphoglycerate kinase-encoding genes mediate developmental regulation. *Gene.* 1995;162(1):153–6.
- Koley NG, Franklin JB, Carmi S, Shi H, Michaeli S, Tschudi C. The transcriptome of the human pathogen *Trypanosoma brucei* at single-nucleotide resolution. *PLoS Pathog.* 2010;6(9):e1001090.
- Rudenko G, Blundell PA, Taylor MC, Kieft R, Borst P. VSG gene expression site control in insect form *Trypanosoma brucei*. *EMBO J.* 1994;13(22):5470–82.

35. Huang W, Li L, Myers JR, Marth GT. ART: a next-generation sequencing read simulator. *Bioinformatics*. 2012;28(4):593–4.
36. Graham VS, Barry JD. Is point mutagenesis a mechanism for antigenic variation in *Trypanosoma brucei*? *Mol Biochem Parasitol*. 1996;79(1):35–45.
37. Lu Y, Hall T, Gay LS, Donelson JE. Point mutations are associated with a gene duplication leading to the bloodstream reexpression of a trypanosome metacyclic VSG. *Cell*. 1993;72(3):397–406.
38. Rice-Ficht AC, Chen KK, Donelson JE. Point mutations during generation of expression-linked extra copy of trypanosome surface glycoprotein gene. *Nature*. 1982;298(5875):676–9.
39. Glover L, Alford S, Horn D. DNA break site at fragile subtelomeres determines probability and mechanism of antigenic variation in African trypanosomes. *PLoS Pathog*. 2013;9(3):e1003260.
40. Gottesdiener K, Chung HM, Brown SD, Lee MG, Van der Ploeg LH. Characterization of VSG gene expression site promoters and promoter-associated DNA rearrangement events. *Mol Cell Biol*. 1991;11(5):2467–80.
41. Berberof M, Vanhamme L, Tebabi P, Pays A, Jefferies D, Welburn S, Pays E. The 3'-terminal region of the mRNAs for VSG and procyclin can confer stage specificity to gene expression in *Trypanosoma brucei*. *EMBO J*. 1995;14(12):2925–34.
42. Durand-Dubief M, Kohl L, Bastin P. Efficiency and specificity of RNA interference generated by intra- and intermolecular double stranded RNA in *Trypanosoma brucei*. *Mol Biochem Parasitol*. 2003;129(1):11–21.
43. Batram C, Jones NG, Janzen CJ, Markert SM, Engstler M. Expression site attenuation mechanistically links antigenic variation and development in *Trypanosoma brucei*. *eLife*. 2014;3:e02324.
44. Goodwin S, McPherson JD, McCombie WR. Coming of age: ten years of next-generation sequencing technologies. *Nat Rev Genet*. 2016;17(6):333–51.
45. Guizetti J, Scherf A. Silence, activate, poise and switch! mechanisms of antigenic variation in *Plasmodium falciparum*. *Cell Microbiol*. 2013;15(5):718–26.
46. Reynolds D, Hofmeister BT, Cliffe L, Alabady M, Siegel TN, Schmitz RJ, Sabatini R. Histone H3 variant regulates RNA polymerase II transcription termination and dual strand transcription of siRNA loci in *trypanosoma brucei*. *PLoS Genet*. 2016;12(1):e1005758.
47. Pena AC, Pimentel MR, Manso H, Vaz-Drago R, Pinto-Neves D, Aresta-Branco F, Rijo-Ferreira F, Guegan F, Pedro Coelho L, Carmo-Fonseca M, et al. *Trypanosoma brucei* histone H1 inhibits RNA polymerase I transcription and is important for parasite fitness in vivo. *Mol Microbiol*. 2014;93(4):645–63.
48. Nguyen TN, Muller LS, Park SH, Siegel TN, Gunzl A. Promoter occupancy of the basal class I transcription factor A differs strongly between active and silent VSG expression sites in *Trypanosoma brucei*. *Nucleic Acids Res*. 2014;42(5):3164–76.
49. Gottesdiener KM. A new VSG expression site-associated gene (ESAG) in the promoter region of *Trypanosoma brucei* encodes a protein with 10 potential transmembrane domains. *Mol Biochem Parasitol*. 1994;63(1):143–51.
50. Overath P, Czichos J, Haas C. The effect of citrate/cis-aconitate on oxidative metabolism during transformation of *Trypanosoma brucei*. *Eur J Biochem*. 1986;160(1):175–82.
51. Li H, Handsaker B, Wysoker A, Fennell T, Ruan J, Homer N, Marth G, Abecasis G, Durbin R, Genome Project Data Processing S. The sequence alignment/Map format and SAMtools. *Bioinformatics*. 2009;25(16):2078–9.
52. Carver T, Harris SR, Berriman M, Parkhill J, McQuillan JA. Artemis: an integrated platform for visualization and analysis of high-throughput sequence-based experimental data. *Bioinformatics*. 2012;28(4):464–9.
53. Glover L, Alford S, Baker N, Turner DJ, Sanchez-Flores A, Hutchinson S, Hertz-Fowler C, Berriman M, Horn D. Genome-scale RNAi screens for high-throughput phenotyping in bloodstream-form African trypanosomes. *Nat Protoc*. 2015;10(1):106–33.

Submit your next manuscript to BioMed Central and we will help you at every step:

- We accept pre-submission inquiries
- Our selector tool helps you to find the most relevant journal
- We provide round the clock customer support
- Convenient online submission
- Thorough peer review
- Inclusion in PubMed and all major indexing services
- Maximum visibility for your research

Submit your manuscript at  
[www.biomedcentral.com/submit](http://www.biomedcentral.com/submit)

